International Journal of
Turbomachinery
Propulsion and Power

MDPI

Article

Active Turbulence Grid-Controlled Inflow Turbulence and Replication of Heat Exchanger Flow Fields in Fan Applications

Felix Czwielong * and Stefan Becker

Institute for Fluid Mechanics, Friedrich-Alexander University Erlangen-Nuremberg, Cauerstr. 4, 91058 Erlangen, Germany
* Correspondence: felix.czwielong@fau.de

Abstract: A novel active turbulence grid of the Institute of Fluid Mechanics at FAU Erlangen-Nuremberg is introduced. The focus of this grid is not on basic investigations of fluid mechanics, as is usually the case with active turbulence grids, but the generation of defined inflow conditions for axial fans. Thus, by means of the active turbulence grid, individual turbulence characteristics in the flow to the fan can be changed; therefore, fundamental interactions between the flow mechanics at the axial fan and the sound radiation can be analyzed. In addition, the replication of the flow fields of heat exchangers by the active turbulence grid is the focus of the investigations. The investigations showed that it is possible to use the active turbulence grid to generate defined inflow conditions for axial fans. It was also possible to reproduce the heat exchanger flow fields both for the mean turbulence values and for the spatial distributions. It was found that the grid induces tonal components due to the drive motors, but also that the inherent noise has no significant influence on the spectrum of the fans under investigation. Based on selected turbulence characteristics, direct correlations were found between the spatial distribution of the turbulence level and sound radiation at the first blade passing frequency of the axial fan. As the variance of the turbulence level increases, the sound radiation of the tonal components becomes more pronounced. The total sound pressure level, however, is mainly determined by the low-frequency broadband sound. A linear relationship between the spatial mean value of the turbulence level and the total sound pressure level was found for the investigated axial fan.

Keywords: axial fan noise; active turbulence grid; heat exchanger; controlled inflow; inflow turbulence; leading edge noise

Citation: Czwielong, F.; Becker, S. Active Turbulence Grid-Controlled Inflow Turbulence and Replication of Heat Exchanger Flow Fields in Fan Applications. *Int. J. Turbomach. Propuls. Power* **2023**, *8*, 1. https://doi.org/10.3390/ijtpp8010001

Academic Editor: Marcello Manna

Received: 30 August 2022
Revised: 30 November 2022
Accepted: 22 December 2022
Published: 4 January 2023

1. Introduction

Turbulence grids are used in wind tunnels and axial fan test rigs to generate increased turbulence intensities, modified length scales and defined flow fields [1,2]. A distinction is made between active and passive turbulence grids. The passive turbulence grids consist of rigid struts, which generate a defined orifice and blocking of the flow field [3]. Active turbulence grids (ATG), on the other hand, consist of shafts with attached wings called turbulence generators. The shafts are driven by motors located outside the flow. The motors generate a rotational motion, which is transmitted onto the shafts and the turbulence generators. The rotation of the turbulence generators can influence the turbulence intensity, the turbulent length scale and the homogeneity of the flow field [4]. The great advantage of the active turbulence grid is that a large number of different flow conditions can be generated with one grid [5,6]. The turbulence parameters are adjusted by changing the rotational speed of individual shafts. Active turbulence grids have been used since 1991 for fundamental investigations of flows and turbulence properties in wind tunnels [7,8]. They are usually operated in a square channel and the flow generated by the grids is analyzed downstream. In a novel approach an active turbulence grid will be used to replicate real flow fields and to generate variable inflow turbulence for axial fans. Thus, the

high variability in the flow field due to the active turbulence grid is used and investigated in the context of axial fans. Two questions arise from this, which are to be explored by means of this approach. On the one hand, it is to be studied to what extent it is possible to replicate real flow fields of heat exchangers. This also raises the question of how the sound radiation of the fan differs between the real flow field and the imitated flow field. This real-world application of axial fans with suction-side heat exchangers is of particular importance because, on the one hand, they are used in a variety of devices in close proximity to humans, such as heat pumps [9]. On the other hand, it is not yet fully understood why a suction-side heat exchanger can increase the sound radiation of axial fans [10,11]. Additionally, complete CFD simulations of the flow field through heat exchangers are not possible until now [12,13]. If the imitation of real flow fields by means of the ATG would be successful, then in future experimental investigations in the scope of heat pumps and air conditioning it would be possible to avoid cumbersome changes between many heat exchangers. This would save time in research as well as in industrial companies. A second question, which should be answered by means of active grids, is how the physical interactions between inflow turbulence to the axial fans and the resulting sound generation are [14]. With the active turbulence grid, it is possible to adjust the turbulence characteristics of the flow independently, in contrast to rigid turbulence grids. Thus, it has been shown in the literature that at low rotational speeds of the turbulence generators, the integral length scale can be varied while the turbulence level remains constant. On the other hand, at high rotational speeds, it was possible to vary the turbulence level, while the length scale remained unchanged [15]. This feature offers the possibility to investigate the influences of the individual turbulence parameters on the sound pressure spectrum of axial fans and thus to derive a better understanding of the sound generation mechanisms. However, for the use of the active turbulence grid in this context, it must be investigated on the one hand whether a modification of the inflow conditions can occur if a circular duct is arranged behind the square duct of the active turbulence grid. Active turbulence grids have a square shape. Axial fans, on the other hand, require a circular duct. Such a change in the cross-sectional area has so far unexplained effects on the generated turbulence of the active turbulence grid. In other studies with a cross-sectional change applied to axial fans, local turbulence spots were generated which changed the sound radiation at the tonal components of the fan [16]. Furthermore, for the investigation of the sound radiation of axial fans, it must be ensured that the inherent noise of the active turbulence grid is so low that no significant influence on the sound pressure spectrum takes place. Since no acoustic investigations with active turbulence grids have been carried out up to now, no data are available in the literature on the acoustic characteristics. The sound radiation of the active turbulence grid changes with the rotational speed of the turbulence generators. For the correct interpretation of the effects of the flow field on the sound emissions from the axial fans, the sound emission of the grid must be known. This radiation must be taken into account from the very beginning because it represents a distortion quantity and must be reduced as much as possible in the design process of the grid.

The structure of the paper consists of the following. First, the experimental fan used is described and its design parameters are discussed. In a further subchapter, the experimental setups for determining the sound field and for characterizing the inflow conditions are described. Then, the novel active turbulence grid is presented, and the constructional details are discussed in detail. This is followed by a subchapter on the sound radiation of the grid and how this changes as a function of the turbulence generator speed. Proceeding from these constitutive setups, the two questions from the introduction are then addressed and a comparison is made between active turbulence grid and heat exchangers. Subsequently, the basic physical interactions between inlet turbulence and sound radiation in the axial fan are discussed. Both questions are discussed with regard to flow fields and sound radiation in the axial fan. The paper is closed by a summary and conclusion.

2. Axial Fan Design and Experimental Setups

2.1. Forward Skewed Axial Fan

A forward skewed axial fan, which operates in a short duct segment with a diameter of D_{duct} = 500 mm, is used for the investigations. The axial fan, its specific blade energy and its sweep angle are shown in Figure 1. The forward skew increases from an angle of $\lambda = 0°$ at the hub to $\lambda = 55°$ at the blade tip. The total diameter of the fan is D_{fan} = 495 mm, which means that the tip gap is s_{tip} = 2.5 mm. The hub diameter of the fan is D_{hub} = 247.5 mm [17]. As is common in heat exchanger applications, the fan operates within a short inlet nozzle, which causes the tip gap to vary along the axial length of the inlet nozzle. As shown in Figure 1, the fan has $z = 9$ blades and is designed for a flow rate of $\dot{V}$ = 1.4 m^3/s at a rotational speed of n_{fan} = 1486 rpm and a total-to-static pressure rise of p_{fan} = 140 Pa [18]. The blades are based on a NACA 4510 profile and designed according the blade element theory [19]. In the investigations, this axial fan was chosen intentionally because, on the one hand, its forward skew is very similar to the fans currently used in industry and, on the other hand, it is very well documented in the literature. The precise knowledge of the behavior of the axial fan in inflow turbulence makes it possible to better classify effects caused by the disturbed inflow conditions of the ATG and to better understand and interpret the physical effects. The aerodynamic and aeroacoustics characteristics of the used axial fan can be found in the literature at various inflow conditions and in interaction with heat exchangers [11,16,19,20].

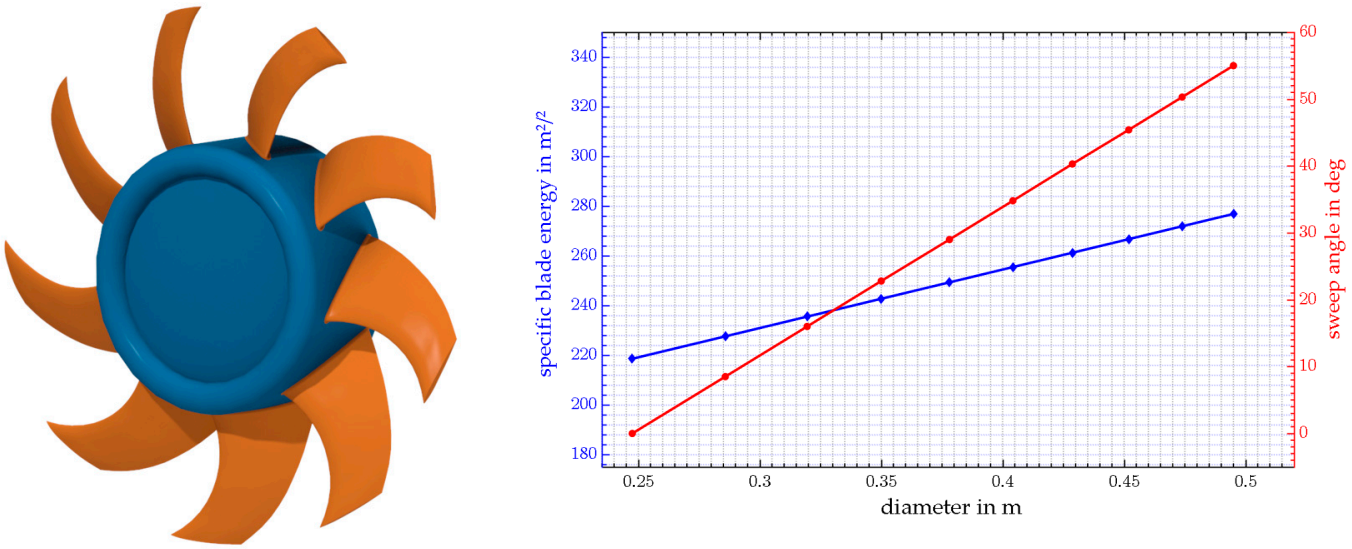

Figure 1. Investigated axial fan and its characteristics. (**a**) CAD representations of the nine bladed forward-skewed axial fan used, and (**b**) the specific blade energy and sweep angle.

2.2. Experimental Setup for the Determination of Sound Emission and Aerodynamic Properties

The sound radiation and the aerodynamic properties of the axial fan are investigated together. For this purpose, the axial fan is installed in the axial fan test rig of the Friedrich-Alexander University Erlangen (see Figure 2). The operating point of the fan can be adjusted by means of a butterfly throttle and an auxiliary fan. The volume flow can be measured with a standardized volume flow measuring device at the inlet. Within the non-reflecting chamber, which is located on the suction side of the test fan, the pressure build-up between the suction side and the ambient pressure is measured. Additionally, within this chamber, the sound radiation of the fan is recorded by five free-field microphones from B&K. The microphones are placed at a distance of one meter from the axial fan. They are located

on a hemisphere, with one microphone directly on the axis of rotation of the fan. Two additional microphones are arranged in $\varphi = 22.5°$ angular segments on a horizontal and a vertical circular arc. The microphones record the acoustic pressure at a sampling rate of $f_s = 48$ kHz for a duration of $t = 30$ s. The speed and torque of the fan can be monitored via the shaft drive, which is located on the pressure side. The pressure, flow rate, rotational speed, torque, density and temperature are recorded at a sampling rate of $f_s = 1$ kHz for $t = 10$ s. Heat exchangers or the active turbulence grid can be positioned in front of the axial fan. Thus, the influence of different inflow conditions on the aerodynamic and acoustic properties of the fan can be investigated.

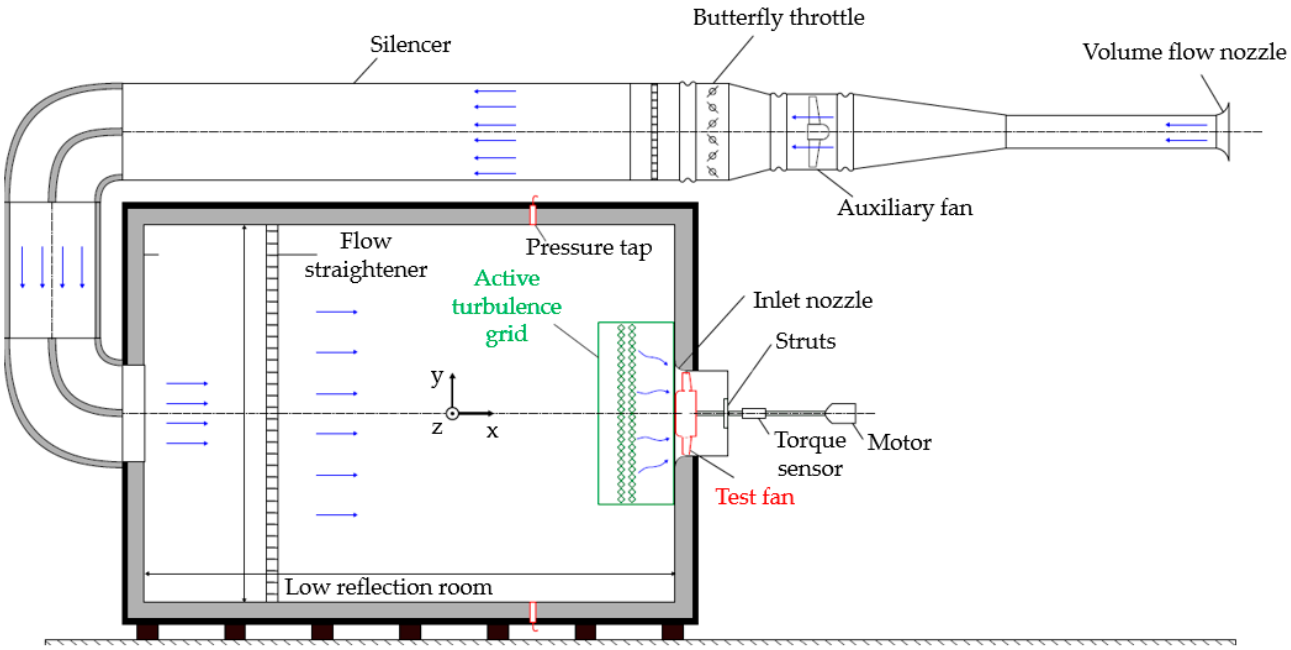

Figure 2. Schematic representation of the axial fan test rig of the LSTM-Erlangen with installed axial fan and active turbulence grid. Design according to DIN EN ISO 5801 [21].

2.3. Determination of Inflow Turbulence and Turbulence Parameters

The inflow conditions to the axial fan are determined at the position where the leading edge of the axial fan is located. At the leading edge, the fan interacts directly with inflow turbulence, and dominant sound sources are generated there, which emit sound primarily in the broadband, low-frequency range [22,23]. The sound source can be attributed to pressure fluctuations at the surface. Since the fan blades block the way to the measuring plane, the fan is replaced by a bladeless hub for the investigation of the flow field [24]. The flow field is determined by means of 3D hot-wire anemometry [25]. For this purpose, one third of a circular segment is measured inside the duct. A total of 80 measuring points with equidistant spacing are distributed in this circular segment (see Figure 3). The measuring points are accessed via a traverse from the pressure side. For each measuring point, the flow velocities in the three spatial directions are measured at a sampling rate of $f_s = 48$ kHz for a period of $t = 30$ s [12,16]. The hot-wire system used, manufactured by Dantec, is calibrated before the measurements [26]. From the data of the flow velocity $u_j(x_i, t)$ the fluctuations of the flow velocity $u'_j(x_i, t)$ can be calculated by Equation (1). $\overline{u}_j(x_i)$ is the time average value of one flow component [27].

$$u'_j(x_i, t) = u_j(x_i, t) - \overline{u}_j(x_i) \tag{1}$$

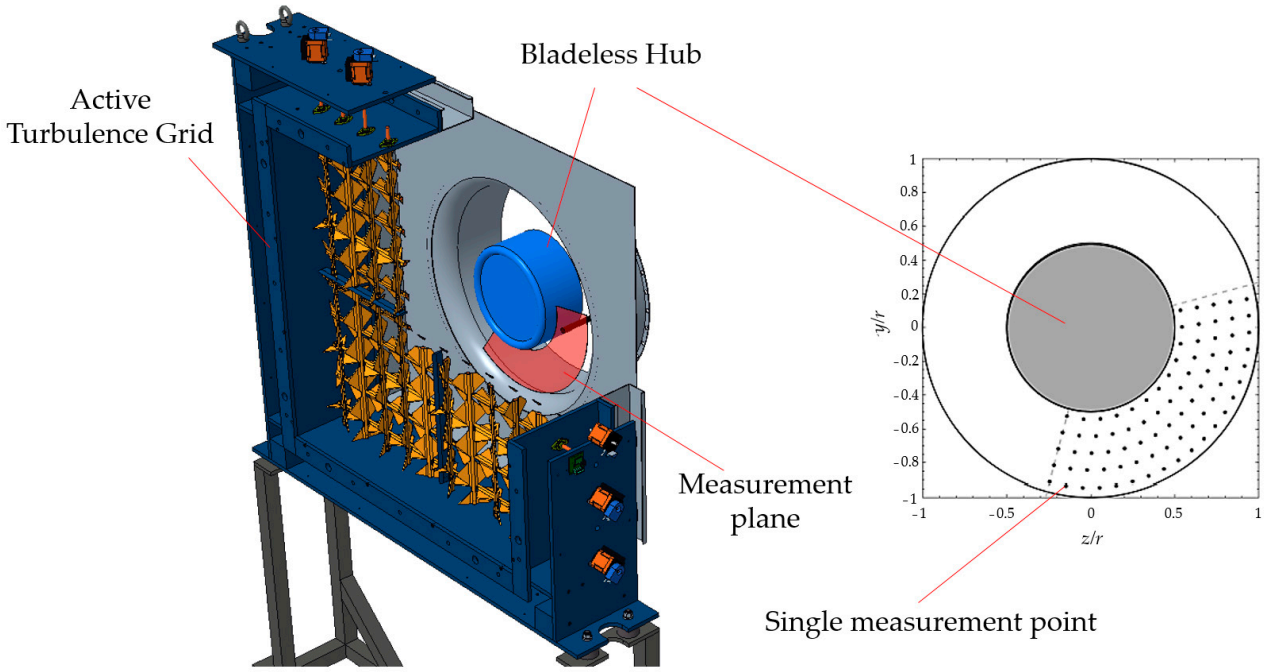

Figure 3. Sectional view of the active turbulence grid with bladeless hub and measuring plane for the hot-wire measurements.

With these, the global turbulence intensity can be calculated based on Equation (2). In this context, the global turbulence intensity Tu_{glo} means that turbulent fluctuations are related to the spatial mean value of the main flow component $\overline{u_{x1}}$ for all 80 measurement points [11].

$$Tu_{glo} = \frac{\sqrt{\frac{1}{3} \cdot \left(\overline{u'^2_{x1}} + \overline{u'^2_{x2}} + \overline{u'^2_{x3}}\right)}}{\overline{u_{x1}}} \tag{2}$$

The integral length scale of the turbulent flow is determined per measurement point from the time data of the main flow velocity. In this case, the length scale is calculated from the energy spectrum $E(f)$ according to Equation (3) and the approach of El-Gabry et al. [28].

$$\Lambda = \left[\frac{E(f) \cdot \overline{u_{x1}}}{4 \cdot \overline{u'^2_{x1}}}\right]_{f \to 0} \tag{3}$$

This procedure refers to isotropic flows, but according to Kurian et al. [29] it can also be used for not completely ideal isotropic flows. The calculation of the integral length scale on the basis of autocorrelation is not an option in these investigations with active turbulence grid. Due to the small distance between the measuring plane and the ATG and the rotation of the turbulence generators, cyclic components are included in the flow data. These would lead to the autocorrelation being a function of the rotational speed of the turbulence generators and thus the length scale would be calculated incorrectly. In addition to these basic parameters of the turbulence theory, a new parameter is presented in this paper, which should provide further insight into the interaction between the axial fan and the flow field. For this purpose, the formula of the variance σ^2 according to Equation (4) is applied to the time average values of the turbulence intensity Tu and the length scale Λ per measuring point (see Equations (5) and (6)). This results in a spatial variance, which combines the temporal and spatial data from the flow field into one value.

$$\sigma^2 = \frac{1}{n-1} \sum_{k=1}^{n} \left(X_k - \overline{X}\right)^2 \tag{4}$$

$$\sigma_{Tu}{}^2 = \frac{1}{n-1}\sum_{k=1}^{n}\left(Tu_k - \overline{Tu}\right)^2 \tag{5}$$

$$\sigma_{\Lambda}{}^2 = \frac{1}{n-1}\sum_{k=1}^{n}\left(\Lambda_k - \overline{\Lambda}\right)^2 \tag{6}$$

3. Active Turbulence Grid

3.1. Constructional Design of the Active Turbulence Grid

An active turbulence grid is used to generate defined inflow conditions. The basic form of the grid is shown as CAD in Figure 4. The turbulence generators, which are shown in orange in the center, are in the closed state, i.e., the maximum blocking of the grid is present. The basic structure of the grid consists of an outer frame and an inner frame, through which the flow passes. The drive motors and their controls are located on the outer frame. A total of 20 stepper motors are used, which are equipped with encoders and heat sinks. Vibration damping couplings are attached to the stepper motors. These couplings reduce the vibrations on the shaft, which are generated by the stepper motor. The outer frame is mounted on vibration dampers. The stepper motors and the space between the inner and outer frames are shielded by foam and motor enclosures so that as little sound as possible can be emitted to the outside from these components.

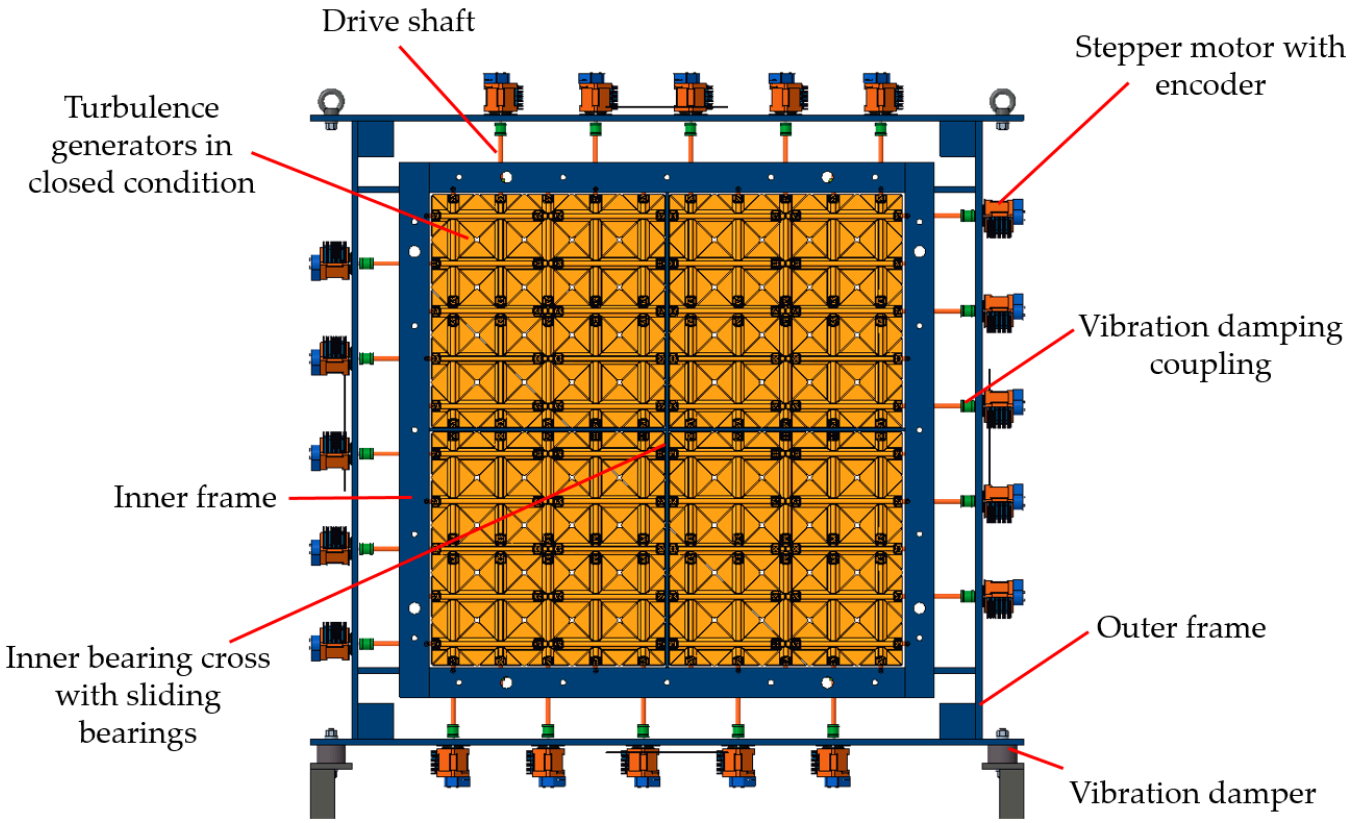

Figure 4. Schematic representation of the basic structure of the active turbulence grid.

Figure 5 shows a partial section of the active turbulence grid, where the flange bearings are visible. These are located outside the flow on the inner frame and guide the shafts on which the turbulence generators are located. In the center of the flow field, the shafts are additionally supported by sliding bearings, which have vibration damping properties. The center cross is designed as a symmetrical airfoil. This prevents stall at the center cross, which is necessary for stability reasons. As shown in Figure 5, there is a front and a rear row of turbulence generators. After the turbulence generators are 3D printed and slid over the shaft to be centered, there must be a gap between the vertical and horizontal axes. Both

the horizontal and vertical axes are positioned 6.5 mm off center. Thus, the shafts have a distance of 13 mm from each other in flow direction.

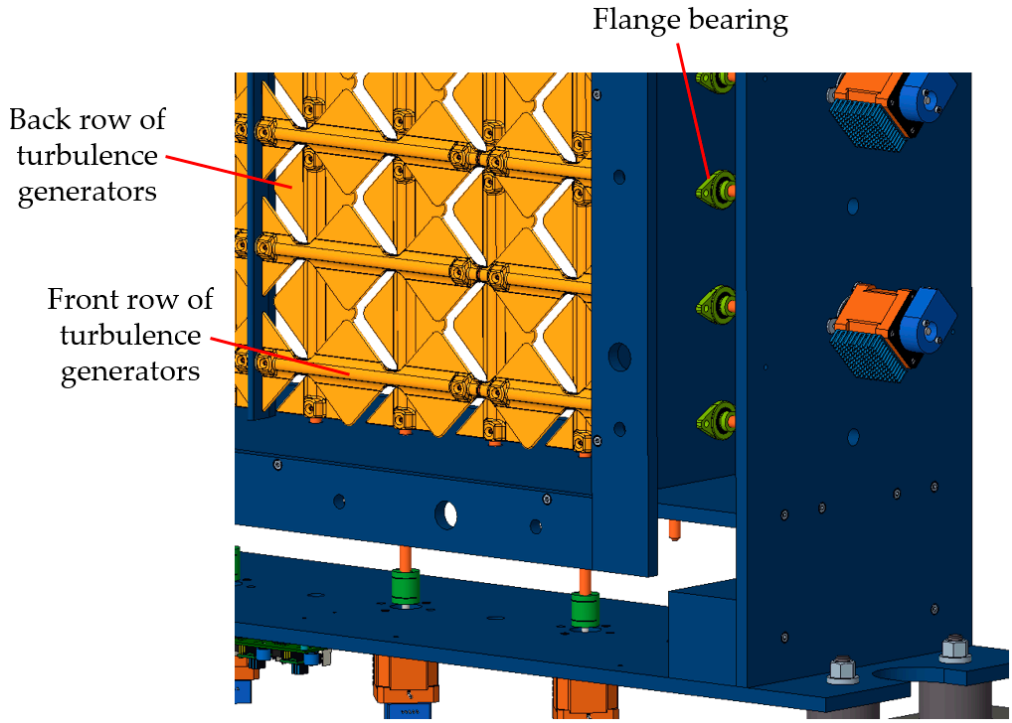

Figure 5. Partial view of the active turbulence grid, in which the distance between the two rows of turbulence generators can be seen.

Figure 6 illustrates a turbulence generator with shaft. The turbulence generators are square wings, which are located on the shaft. Each 2.5 wings consist of a joint 3D printed part and can be slid onto the shaft and fixed there by means of screws. The inner frame of the active turbulence grid, where the flow passes through, has square dimensions of 800 × 800 mm. The turbulence generators are shortened by a total of 7.5 mm. For this reason, there is a space of 3.75 mm between the two ends of a turbulence generator shaft and the respective frame wall. This clearance, as well as the distance between the horizontal and vertical axes, is necessary so that the turbulence generators do not drag or collide with each other during operation. By means of the individually controllable stepper motors, each of the 20 drive shafts, with the turbulence generators located on them, can be adjusted independently of each other. These settings include the direction of rotation, the rotational speed, the start position, the acceleration, a standstill position or relative movements to other drive shafts.

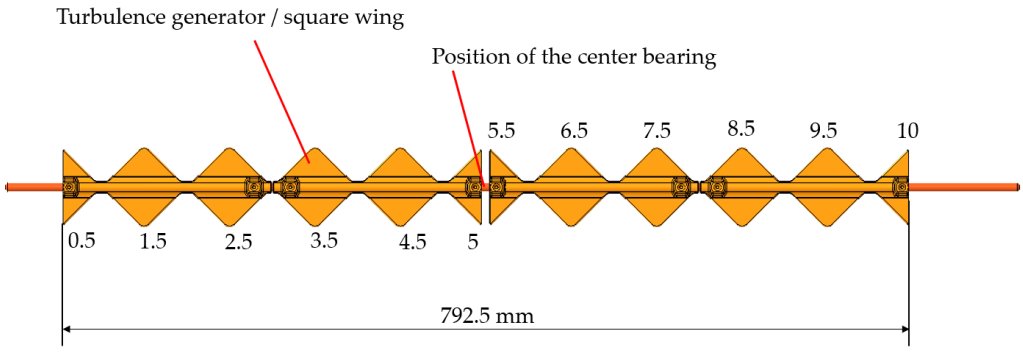

Figure 6. Detail of a single drive shaft with turbulence generators attached.

The number of individual shafts determines the mesh size of the active turbulence grid, which is M = 80 mm. The axial length of the active turbulence grid is L = 260 mm. By means of adapters on the inner frame, the square channel of the grid can be extended as desired both at the front and at the rear. In the tests presented here, a total length of L = 330 mm was selected, with an extension of 70 mm in the direction of flow (see Figure 3). The dimensions of the heat exchanger, which also plays a role in these investigations, are 800 × 800 × 330 mm, which thus corresponds to the same flow area and expansion as with the ATG. After the housing of the grid there is a transition to a circular duct with D = 500 mm diameter [11,16]. The transition is realized by an inlet nozzle. The axial fan to be investigated is operated in the round duct. If the axial fan is installed, the distance between it and the center plane of the two rotation planes of the active turbulence grid is d = 200 mm.

Figure 7 shows the active turbulence grid within the anechoic chamber of the axial fan test rig at the University of Erlangen-Nuremberg [30]. The active turbulence grid is shown in its basic shape without sound enclosure. Additionally, the five free-field microphones for measuring the sound radiation on the suction side are visible.

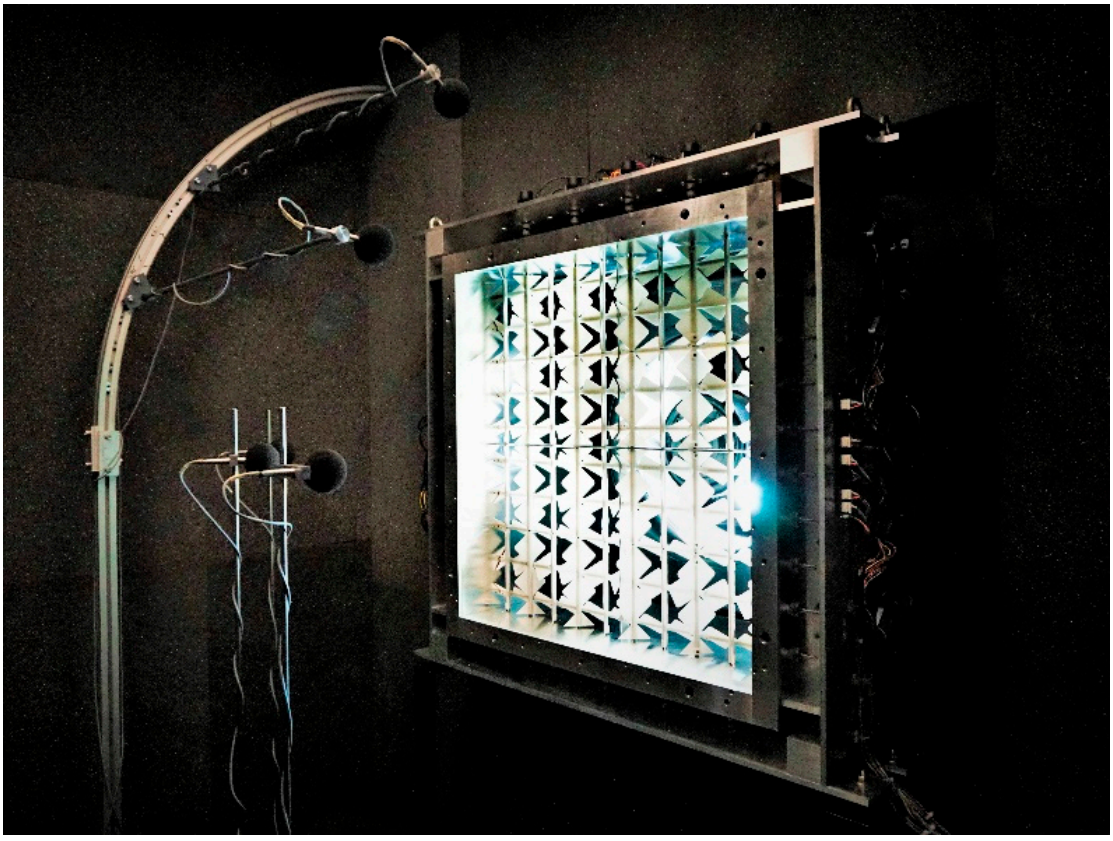

Figure 7. The active trubulence grid inside the anechoic chamber.

3.2. Intrinsic Noise of the Active Turbulence Grid

In order to better separate the acoustic influence of the active turbulence grid on the measurement results of the sound pressure from the axial fans under investigation, the inherent noise of the active turbulence grid was determined. The noise is low enough that it can be assumed that the intrinsic noise of the grid is masked by the fan noise [14,31]. Figure 8 displays a comparison between the sound radiation of the axial fan with an empty box in front and selected operating conditions of the ATG.

The spectra in Figure 8 are the inherent noise of the active turbulence grid at constant speeds. In this case, all motors rotate at the same speed and the grid blockage is constantly set to 50% blockage. A blockage of 50% is achieved by starting half of the turbulence

generators at 90° offset to the others. Operating modes in which all shafts rotate at the same speed are usually the noisiest. Thus, the case with the maximum speed of 800 rpm of the ATG is also the acoustically worst case. As a reference value, the noise of the axial fan is chosen when an empty box (an empty heat exchanger housing) is positioned in front of the axial fan on the suction side. With the ATG, a corresponding housing is always positioned in front of the axial fan due to the inner frame. Thus, this case represents a better comparison case, than the free inflow, because so also the influence of the changed directional characteristics is considered [32]. Only for the maximum speed of 800 rpm are there a few frequencies at which the spectrum of the axial fan does not mask the noise of the ATG. The overall sound pressure level is 11 dB away from the ATG's inherent noise at 800 rpm, far enough away that it can be assumed that the fan's sound radiation is not affected by the inherent noise of the turbulence grid. In the high-frequency range, tonal components appear individually through the spectrum of the axial fan.

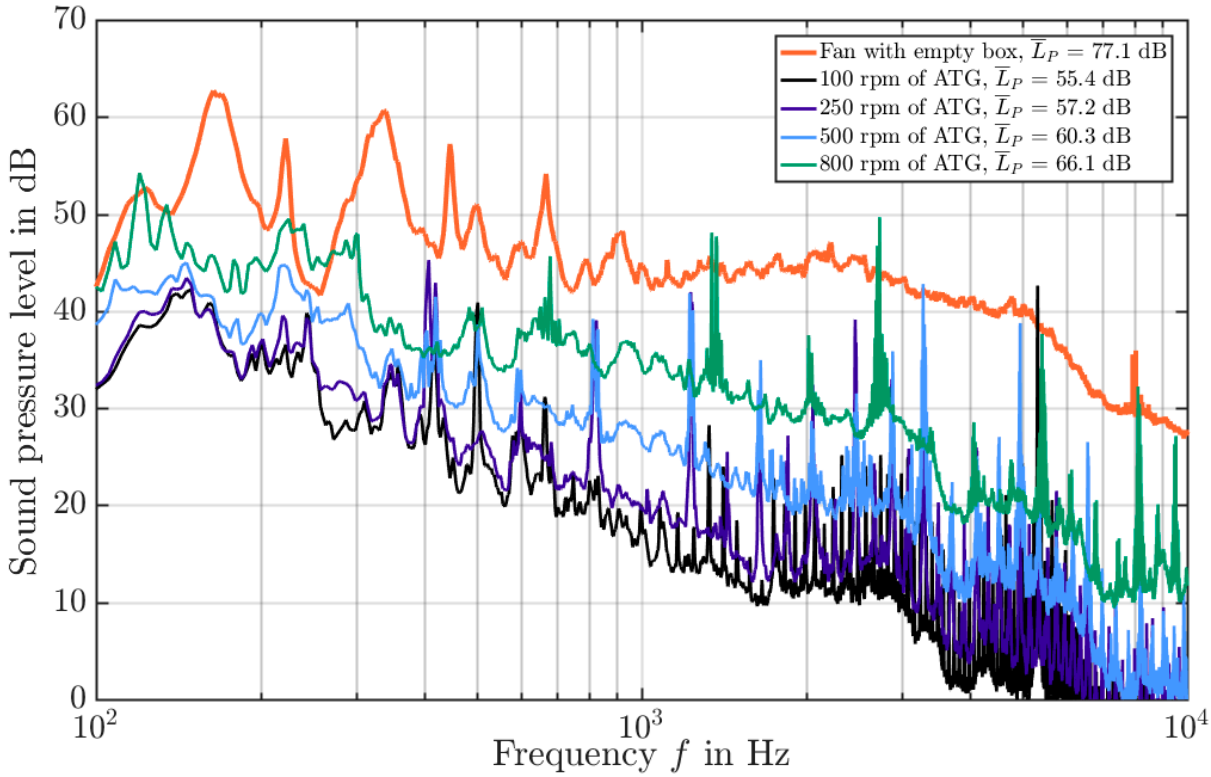

Figure 8. Comparison of the sound pressure spectra of the axial fan with the inherent noise of the ATG.

Through a run-up and a resulting Campbell plot (see Figure 9), it can also be determined that the tonal components generated by the active grid are related to the speed of the shafts. In addition, the linear relationship between the tonal components in the sound spectrum and the motor speed is related to the steps and micro steps of the motors used. These perform 200 steps and 3200 micro steps per revolution. The corresponding sound radiation of the tonal components can be calculated using Equation (7). The rotational speed n and the step size δ goes into the calculation of the respective frequency. The tonal sound radiation due to the microstep is the 16th harmonic (k = 16) of the fundamental frequency.

$$f_k = k \cdot \frac{n}{60} \cdot \frac{360^\circ}{\delta};\ k \in \mathbb{N} \tag{7}$$

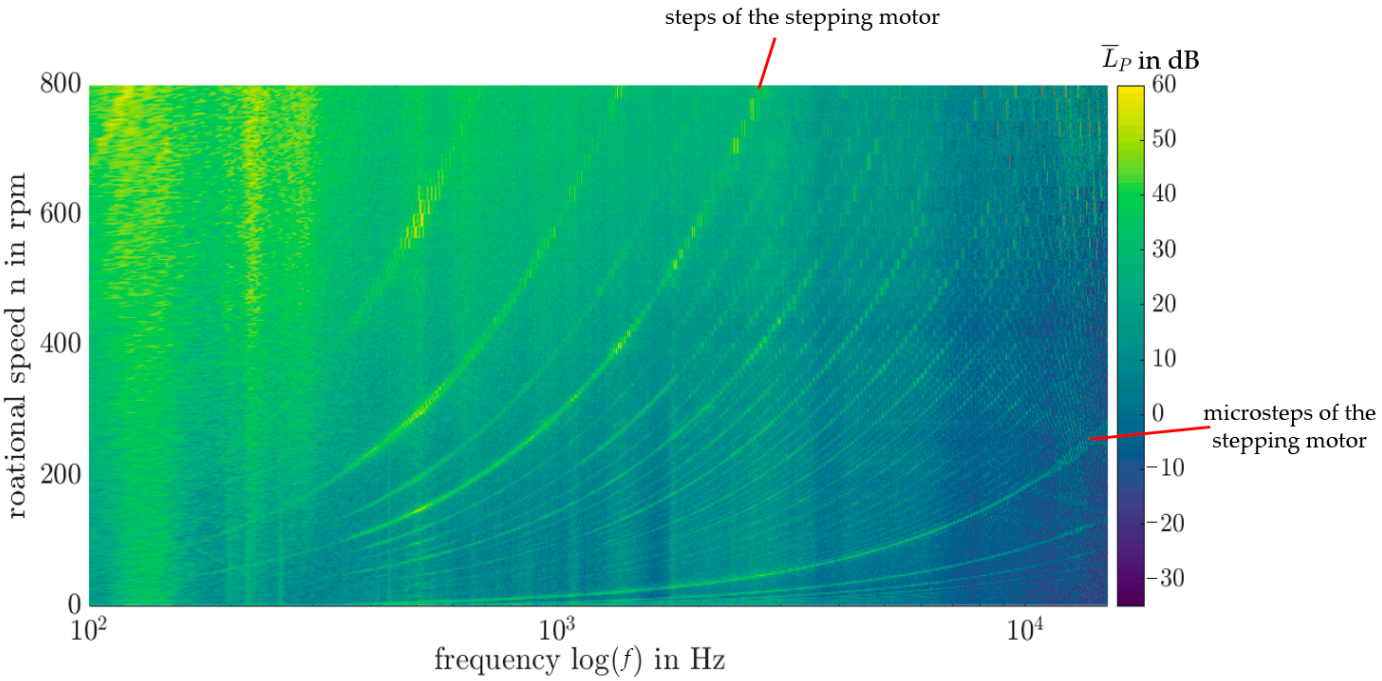

Figure 9. Campbell-plot of the self-induced noise of the active turbulence grid.

4. Controlled Inflow Turbulence and Flow Field Replication of Heat Exchangers

4.1. Generation of Defined Inflow Conditions

In many literatures in the field of sound radiation from axial fans, the inflow conditions are defined by spatial mean values of turbulence intensity and length scale [33,34]. These two values are also used for empirical sound prediction models for the axial fan and are essential for its sound radiation [35,36]. Thus, when the spatial mean values of these two quantities are plotted against each other, a characteristic map for the inflow conditions of the axial fan can be generated. In Figure 10, the global values of turbulence level and integral length scale are plotted in a characteristic map. Different operating modes of the active turbulence grid are shown with red dots in the map. The black squares are representative of four different heat exchangers with the dimensions of 800 × 800 mm. The distribution of the red dots shows that the active turbulence grid can vary the turbulence level in the range of [6.7%; 16.3%] and the length scale in the range of [3.7 mm; 36.2 mm]. In addition, a kind of pareto front [37] is recognizable in the measurement data. In total, more than 60 different operating conditions with different flow fields were generated with an active turbulence grid. Since at this point the basic functionality of the grid for the application in the field of turbulent inflow conditions of axial fans should be demonstrated, the individual flow fields and how they were generated will not be discussed. As different operating modes were used rigid modes, i.e., without rotation of shafts, uniform modes, where all shafts rotate at the same speed, staged modes, where different shafts have different speeds, and partially rotating modes, where only one part of the shaft rotates while the other part is stationary. The relationship that at constant slow speed the length scale can be adjusted and at constant high speed the turbulence intensity can be controlled independently, which is described in the literature [15], could also be found in this application. Thus, the characteristic map of the active turbulence grid (see Figure 10) proves that, for example, the length scale can be varied in the region of Tu_{glo} = 14% turbulence level, whereas the average turbulence level remains almost constant at this value. At a length scale of about Λ = 5 mm, the opposite pattern is seen. In this range, the turbulence level can be changed while the length scale remains constant. Thus, the active turbulence grid allows a separation of the influences of the different turbulence characteristics on the sound spectrum of axial fans to be investigated independently of each other.

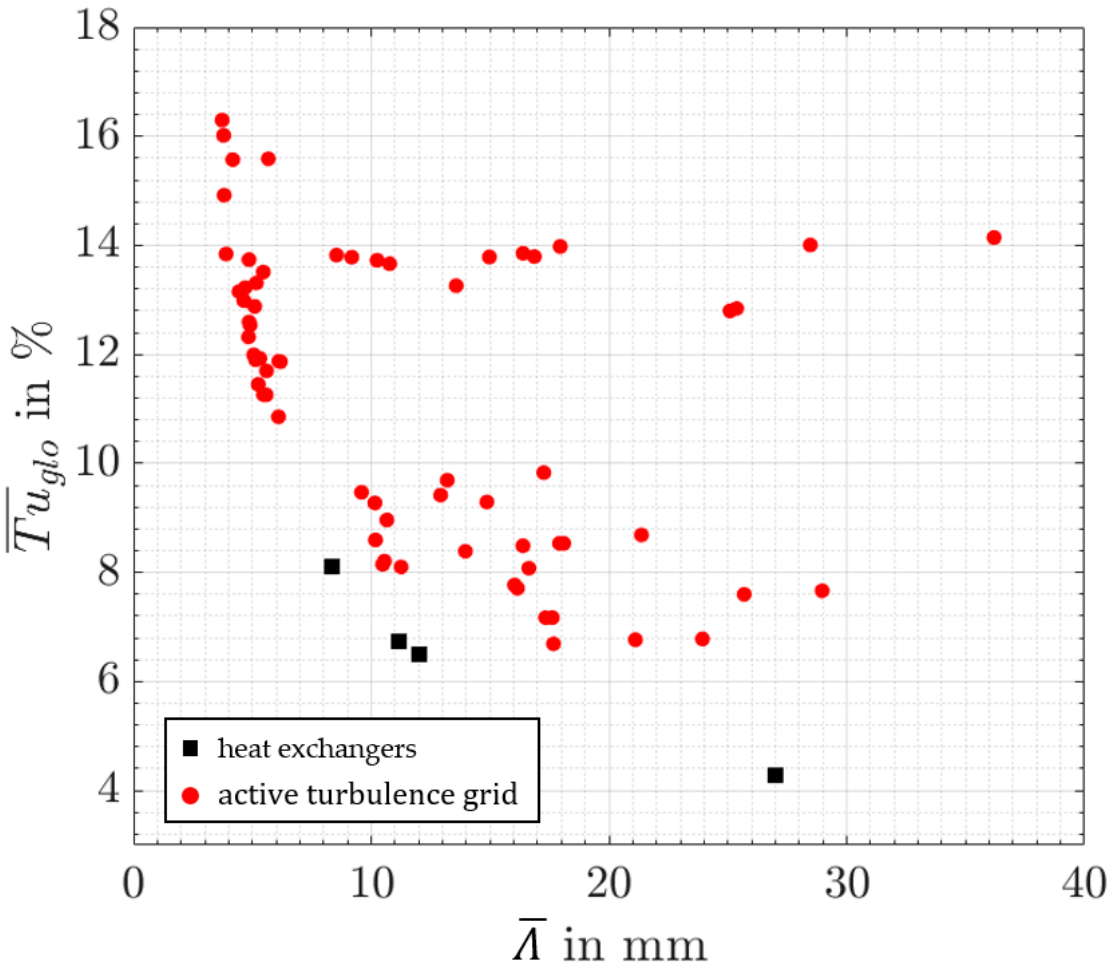

Figure 10. Characteristic map of the induced turbulence characteristics of heat exchangers and different active turbulence grid modes. Black squares are measured values of the heat exchangers, red circles are individual operating modes of the ATG.

4.2. Reproduction of the Flow Fields of Heat Exchangers

The four heat exchangers from Figure 10 are industrial devices, which are used, for example, in heat pumps or refrigeration systems. The turbulence intensity decreases with decreasing pipe diameter. Thus, the heat exchanger with the highest turbulence intensity has a tube diameter of 12 mm, the two black squares in the middle have a tube diameter of 9.52 mm, and the heat exchanger with the lowest turbulence intensity has a tube diameter of 5 mm. A detailed description of the heat exchangers can be found in the literature [16]. Especially the heat exchanger with the highest turbulence level can be reproduced very well in the mean values by the active turbulence grid. Here, the mean values in the length scale between heat exchanger and active turbulence grid deviate by only 2 mm. For the two heat exchangers in the turbulence range of 6.5%, the active turbulence grid can reproduce the turbulence level, but the length scale deviates by 6 mm. The heat exchanger with the low turbulence level of 4.3% cannot yet be reproduced by the active turbulence grid so far. Further investigations will show whether this range can be achieved in the map via other operating modes.

Since the active turbulence grid seems to be able to reproduce the average flow values of heat exchangers, a comparison between the flow field downstream of a heat exchanger (Tu_{glo} = 8.12%, Λ = 8.34 mm) and the most similar operating mode of the active turbulence grid (Tu_{glo} = 8.15%, Λ = 10.48 mm) is shown in Figure 11. In addition, the flow pattern of a free inlet flow is shown as a reference (Figure 11c).

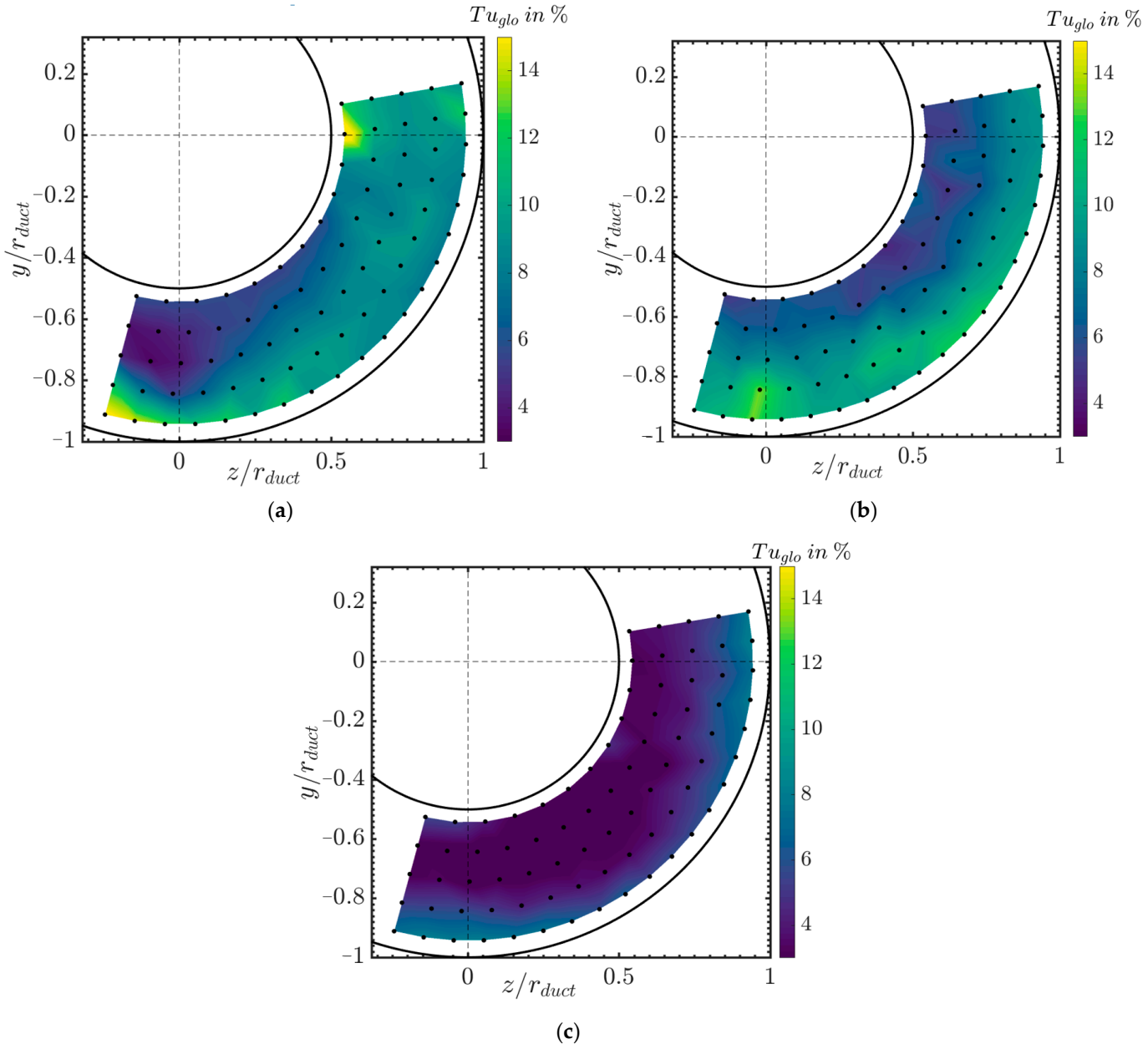

Figure 11. Comparison of the turbulence level between heat exchanger, imitated flow field by active turbulence grid and the undisturbed inflow at a volume flow rate of $\dot{V}$ = 1.4 m^3/s. (**a**) Flow field behind a real heat exchanger, (**b**) flow field reproduced by ATG and (**c**) free, undisturbed inflow.

The surface plots of the turbulence level display that flow conditions similar to those of heat exchangers can be created with the active turbulence grid. It is noticeable that the flow field seems to be rotated by 90° in the plots shown. Nevertheless, inhomogeneities in the flow field, which are mainly generated by the square housing of the heat exchanger and the active grid, can be reproduced [16,38]. The two-dimensional distribution of turbulence values also shows similar tendencies. Compared to the free inflow, the turbulence intensity increases through the heat exchanger as well as through the active turbulence grid. The inhomogeneity in the distribution increases in both cases compared to the free inflow.

5. Sound Emissions of Axial Fan and Active Turbulence Grid

5.1. Heat Exchanger and Active Turbulence Grid

The active turbulence grid is not only intended to reproduce the flow field of the heat exchangers, but also to reproduce the sound radiation of axial fans positioned downstream of heat exchangers as best as possible. The sound pressure spectrum is used to evaluate the sound emissions on the suction side of the axial fans. A comparison of the active turbulence grid and the heat exchanger should only be made at the operating point at which the flow data are available. A change in the flow velocity within the active turbulence grid leads to a change in the grid Reynolds number, which in turn changes the turbulence level and the length scale generated by the grid [15]. Figure 12 shows the sound pressure spectrum of the forward skewed axial fan at the design point. Here, the spectrum that is induced when a heat exchanger is placed in front of the axial fan and the spectrum when an active turbulence grid generates similar flow conditions are presented. In both cases, the sound measurements were made inside the anechoic chamber, on the suction side of the axial fan. Accordingly, the sound is influenced during its propagation to the microphones by the heat exchanger or the active turbulence grid, which are also located on the suction side of the axial fan. In this operating point there is a difference of 0.7 dB in the overall sound pressure level of the two variants. From this, follows that the overall sound pressure level is reproduced well by means of active turbulence grids. In addition, the sound pressure spectra have similar trends, in which the subharmonic peak and the higher harmonic blade passing frequencies are reproduced. Only the first blade passing frequency (1.BPF) is higher in the case with the active turbulence grid. This could be due to a higher turbulence spot in the flow field, which is not detected by the measurement in the third segment of the duct [16]. At higher frequencies, the heat exchanger consistently induces a lower sound pressure level. However, this difference is not due to the flow field, but to the sound guiding properties of the heat exchanger. Czwielong et al. [32] have identified that the differences in the high frequencies are due to the periodic arrangement of the coolant tubes in the heat exchanger and to the thermoviscous losses due to the high number of cooling fins. Thus, the differences in the high frequency range can be corrected by knowledge of the heat exchanger's sound transmission characteristics.

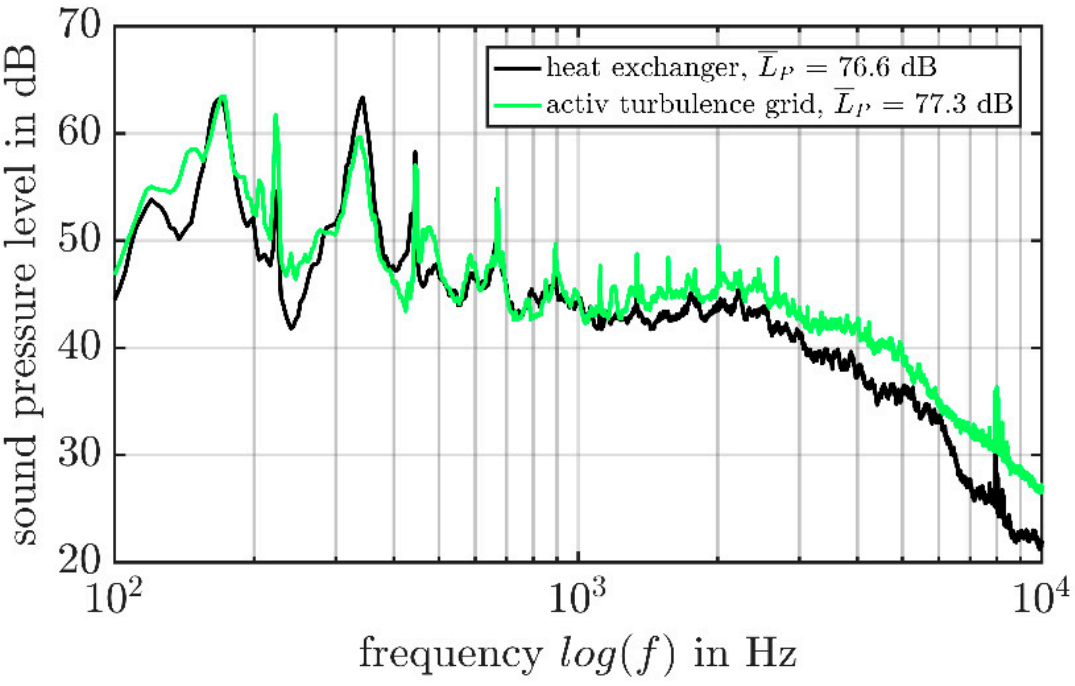

Figure 12. Sound pressure spectra of the heat exchanger (Tu_{glo} = 8.12%, Λ = 8.34 mm) and the active turbulence grid (Tu_{glo} = 8.15%, Λ = 10.48 mm) at the design point ($\dot{V}$ = 1.4 m^3/s).

5.2. Fundamental Investigations between Flow Field and Axial Fan Sound Radiation

Based on the flow field investigations, the sound emissions of the axial fan were investigated in nineteen selected operating modes of the active turbulence grid. The sound pressure spectra obtained at the design point were analyzed, for example, on the basis of the sound radiation at the first blade passing frequency (1.BPF = $z = n/60$ = 222.9 Hz, with z = 9 blades and n = 1486 rpm) and the total sound pressure level up to 1 kHz, which is mainly determined by the low-frequency broadband sound. The first blade passing frequency is often a dominant tonal component in the sound pressure spectrum of low-pressure axial fans and should be kept as low as possible so that the fan noise is not perceived as annoying [39]. Figure 13a displays the relationship between the acoustic emission of the axial fan at the first blade passing frequency and the spatial mean value of the turbulence level. From the data distribution, it can be concluded that no correlation between the mean spatial turbulence level and the sound emission at the first BPF can be found. This indicates that it is often not sufficient to give only mean turbulence levels when the sound pressure spectra of axial fans are discussed in the literature. Figure 13b displays the relationship between the first BPF and the spatial variance of the turbulence level. It can be clearly identified that as the variance increases, the acoustic radiation of the axial fan increases at the first BPF. A linear fit is given as a red dashed line in the plot. Equation (8) is the equation of the linear fit curve, in which the turbulence level in percent is inserted. The coefficient of determination has a value of R^2 = 77.66% for the fit. The relationship between the total sound pressure level between 0.1 kHz and 1 kHz, which is mainly determined by the broadband noise at the leading edge of the fan, and the spatial mean value as well as the spatial variance of the turbulence intensity is shown in Figure 13c,d.

For the total sound pressure level, no linear relationship to the spatial variance of the turbulence intensity can be found. In fact, the total sound pressure level remains almost independent of this parameter because a horizontal tendency develops. However, the total sound pressure level is influenced to a certain extent by the spatial mean value of the turbulence intensity. Here, a linear fit can be performed, which is given in Equation (9) and has a value of R^2 = 34.10%. The fit is shown as a dashed red line in Figure 13c.

$$SPL_{1.BFF,Fit} = 0.8656 \cdot {\sigma_{Tu}}^2 + 57.2 \text{ dB} \quad (8)$$

$$OSPL_{1kHz,Fit} = 0.1195 \cdot \overline{Tu} + 74.25 \text{ dB} \quad (9)$$

The existence of a linear relationship between the sound radiation at the first BPF and the spatial variance of the turbulence level indicates that the knowledge and specification of spatial parameters is critical for the understanding of the sound emission of axial fans. The spatial variance offers the possibility not only to represent discontinuities in the turbulence level by surface plots but also to describe these discontinuities in a statistical value. A high spatial variance means that spatial gradients in the turbulence level are present. When the fan blade moves through these gradients, it experiences a change in the blade forces, which in turn leads to a change in the sound radiation of the 1.BPF. Low values of the spatial variance of the turbulence level indicate a homogeneously distributed turbulence level. The fan blade moves through fewer gradients; therefore, experiences fewer changes in blade forces as it rotates through the flow field. As a result, the sound emission decreases at the 1.BPF. In heat exchanger applications, strong inhomogeneities in the flow field may occur. To minimize sound radiation at the 1.BPF, these inhomogeneities in the flow field should be avoided as far as possible.

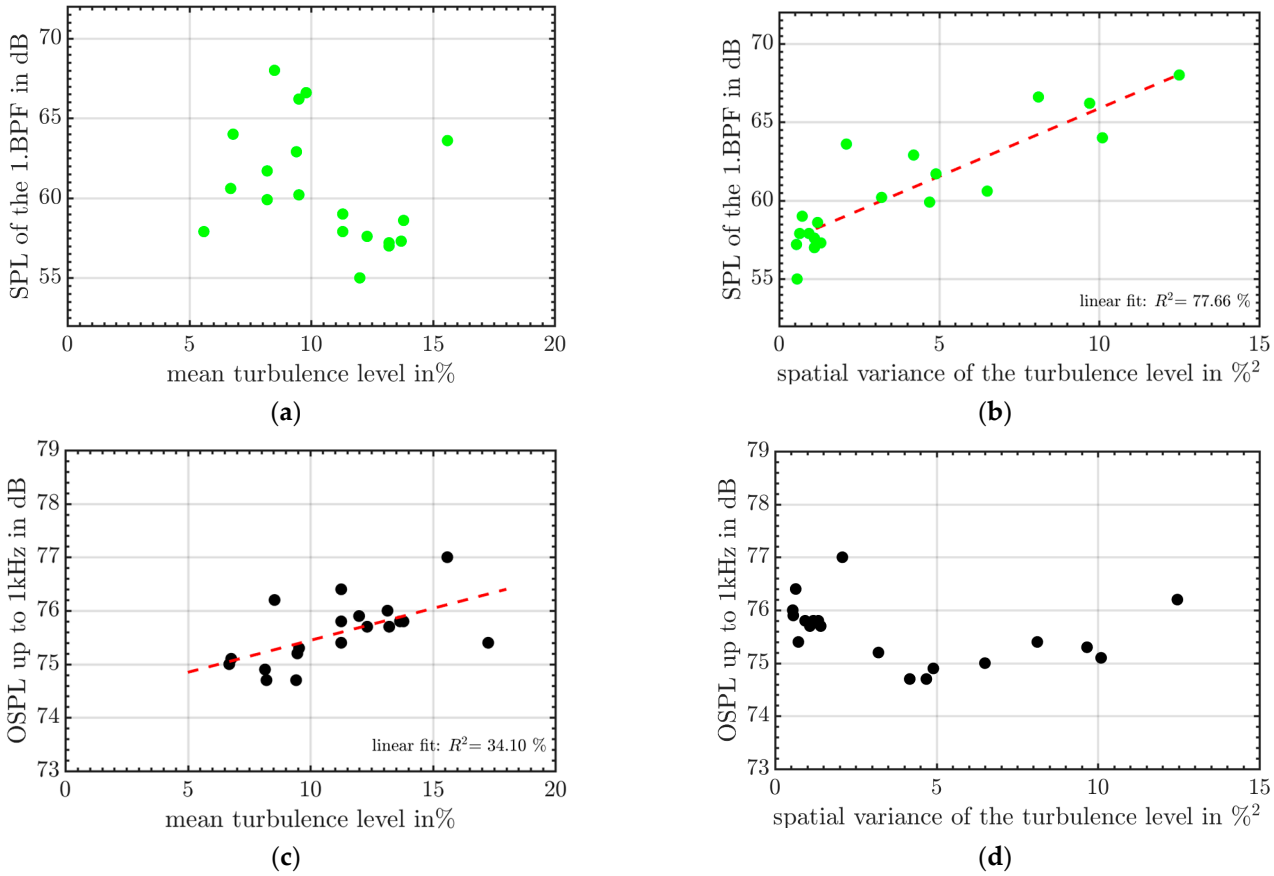

Figure 13. Influence of spatial mean turbulence intensity and spatial variance of turbulence intensity on sound radiation of axial fan at first blade passing frequency (1.BPF) and total sound pressure level between 0.1 kHz and 1 kHz. (**a**) BPF in dependence of the spatial mean value of the turbulence intensity, (**b**) BPF as a function of spatial variance of turbulence intensity with linear fit function, (**c**) BPF as a function of the spatial mean value of the turbulence intensity with linear fit function and (**d**) OSPL in dependence of the spatial variance of turbulence intensity.

6. Conclusions

An active turbulence grid was presented, which can be used for the generation of inflow turbulence of axial fans. The acoustic characterization of the active turbulence grid showed that the inherent noise of the grid is low enough and no significant influence on the sound pressure spectra of the axial fans under investigation is to be expected. In addition, it was found that the tonal peaks of the active turbulence grid depend on the rotational speed of the shafts and the number of steps of the stepper motors. On the basis of 3D hot-wire investigations, it was demonstrated that the active turbulence grid can be used to generate a large number of different inflow conditions, and that the mean turbulence characteristics and the spatial turbulence characteristics induced by heat exchangers can be reproduced by means of the active turbulence grid. The sound radiation of the investigated forward skewed axial fan between a heat exchanger and the active turbulence grid, which both induce comparable inflow conditions, also had similar tendencies. Here, differences in the high frequency range could be attributed to the absence of cooling fins. Based on a large number of sound radiation investigations, a linear relationship was found between the sound pressure level at the first blade passing frequency and the spatial variance of the turbulence level. No correlation was found between the sound radiation at the 1. BPF and the spatial mean of the turbulence level. This result indicates on the one hand that the spatial flow field significantly influences the sound radiation of axial fans and on the other hand that for the understanding of the sound generation mechanisms at the axial fan not only mean values are sufficient. However, the total sound pressure level up to 1 kHz did

not depend on the spatial variance of the turbulence level, but on the spatial average of the turbulence level. The derived value of spatial variances of turbulence level and length scale should be considered in future studies on inflow turbulence of axial fans to achieve a better understanding between the sound radiation and the flow field.

Author Contributions: Conceptualization, F.C.; methodology, F.C.; software, F.C.; validation, F.C.; formal analysis, F.C.; investigation, F.C.; resources, S.B.; data curation, F.C.; writing—original draft preparation, F.C.; writing—review and editing, F.C. and S.B.; visualization, F.C.; supervision, S.B.; project administration, F.C. and S.B.; funding acquisition, S.B. All authors have read and agreed to the published version of the manuscript.

Funding: F.C. and S.B. acknowledge support by the Federal Ministry of Economics and Climate Protection (Bundesminesterium für Wirtschaft und Klimaschutz – BMWK) (Forschungskuratorium Maschinenbau e.V.–FKM, AiF-Forschungsvereinigung, Project: Installationseffekte Axial, Grant No. 20659 N/1). Gefördert durch Bundesministerium für Wirtschaft und Klimaschutz aufgrund eines Beschlusses des Deutschen Bundestages.

Institutional Review Board Statement: Not applicable.

Informed Consent Statement: Not applicable.

Data Availability Statement: The data presented in this study are available on request from the corresponding author.

Acknowledgments: We would like to thank the FLT Project Advisory Committee and the company Thermofin GmbH for their support in the research project.

Conflicts of Interest: The authors declare no conflict of interest.

References

1. Roach, P.E. The generation of nearly isotropic turbulence by means of grids. *Int. J. Heat Fluid Flow* **1987**, *8*, 82–92. [CrossRef]
2. Carolus, T.H.; Stremel, M. Blade surface pressure fluctuations and acoustic radiation from an axial fan rotor due to turbulent inflow. *Acta Acust. United Acust.* **2002**, *88*, 472–482.
3. Lavoie, P.; Djenidi, L.; Antonia, R.A. Effects of initial conditions in decaying turbulence generated by passive grids. *J. Fluid Mech.* **2007**, *585*, 395–420. [CrossRef]
4. Makita, H.; Sassa, K. Active Turbulence Generation in a Laboratory Wind Tunnel. In *Advances in Turbulence*; Springer: Berlin, Germany, 1991; Volume 3, pp. 497–505. [CrossRef]
5. Thormann, A.; Meneveau, C. Decaying turbulence in the presence of a shearless uniform kinetic energy gradient. *J. Turbul.* **2015**, *16*, 442–459. [CrossRef]
6. Larssen, J.V.; Devenport, W.J. On the generation of large-scale homogeneous turbulence. *Exp. Fluids* **2011**, *50*, 1207–1223. [CrossRef]
7. Mydlarski, L. A turbulent quarter century of active grids: From Makita (1991) to the present. *Fluid Dyn. Res.* **2017**, *46*, 061401. [CrossRef]
8. Hideharu, M. Realization of a large-scale turbulence field in a small wind tunnel. *Fluid Dyn. Res.* **1991**, *8*, 53. [CrossRef]
9. Carroll, P.; Chesser, M.; Lyons, P. Air Source Heat Pumps field studies: A systematic literature review. *Renew. Sustain. Energy Rev.* **2020**, *134*, 110275. [CrossRef]
10. Czwielong, F.; Floss, S.; Kaltenbacher, M.; Becker, S. Sound reduction in heat exchanger modules by integrating plate absorbers with sub-millimeter openings. *Acta Acust.* **2021**, *5*, 35. [CrossRef]
11. Czwielong, F.; Krömer, F.; Becker, S. Experimental Investigations of the Sound Emission of Axial Fans Under the Influence of Suction-Side Heat Exchangers. In Proceedings of the 25th AIAA/CEAS Aeroacoustics Conference, Delft, The Netherlands, 20–23 May 2019; p. 2618. [CrossRef]
12. Lucius, A.; Schneider, M.; Schweitzer-De Bortoli, S.; Gerhard, T.; Geyer, T. Aeroacoustic Simulation and Experimental Validation of Sound Emission of an Axial Fan Applied in a Heat Pump. In Proceedings of the 23rd International Congress on Acoustics, Universitätsbibliothek der RWTH Aachen, Aachen, Germany, 9–13 September 2019.
13. Réz, I. Numerische Untersuchung des Luftseitigen Wärmeübergangs und Druckverlustes in Lamellenrohr-Wärmeübertragern mit Verschiedenen Rohrformen. Ph.D. Thesis, Technische Universität Bergakademie Freiberg, Freiberg, Germany, 2004.
14. Czwielong, F.; Becker, S. Aktives Turbulenzgitter—Generierung definierter Zuströmturbulenzen für Axialventilatoren. In Proceedings of the DAGA 2021, Vienna, Austria, 15–18 August 2021.
15. Hearst, R.J.; Lavoie, P. The effect of active grid initial conditions on high Reynolds number turbulence. *Exp. Fluids* **2015**, *56*, 185. [CrossRef]

16. Czwielong, F.; Soldat, J.; Becker, S. On the interactions of the induced flow field of heat exchangers with axial fans. *Exp. Therm. Fluid Sci.* **2022**, *139*, 110697. [CrossRef]
17. Krömer, F.; Müller, J.; Becker, S. Investigation of aeroacoustic properties of low-pressure axial fans with different blade stacking. *AIAA J.* **2018**, *56*, 1507–1518. [CrossRef]
18. Krömer, F.J. *Sound Emission of Low-Pressure Axial Fans Under Distorted Inflow Conditions*; FAU University Press: Boca Raton, FL, USA, 2018. [CrossRef]
19. Pfleiderer, C. *Strömungsmaschinen*; Springer: Berlin, Germany, 2013.
20. Krömer, F.J.; Moreau, S.; Becker, S. Experimental investigation of the interplay between the sound field and the flow field in skewed low-pressure axial fans. *J. Sound Vib.* **2019**, *442*, 220–236. [CrossRef]
21. *DIN EN ISO 5801*; Fans–Performance Testing Using Standardized Airways (ISO 5801: 2007, Including COR 1: 2008), German Version EN ISO 5801. German Institute for Standardization: Berlin, Germany, 2008.
22. Ocker, C.; Geyer, T.F.; Czwielong, F.; Krömer, F.; Pannert, W.; Merkel, M.; Becker, S. Permeable Leading Edges for Airfoil and Fan Noise Reduction in Disturbed Inflow. *AIAA J.* **2021**, *59*, 4969–4986. [CrossRef]
23. Moreau, S.; Roger, M. Competing broadband noise mechanisms in low-speed axial fans. *AIAA J.* **2007**, *45*, 48–57. [CrossRef]
24. Carolus, T.; Schneider, M.; Reese, H. Axial flow fan broad-band noise and prediction. *J. Sound Vib.* **2007**, *300*, 50–70. [CrossRef]
25. Bruun, H.H. *Hot-Wire Anemometry: Principles and Signal Analysis*; Oxford Unversity Press: New York, NY, USA, 1996.
26. Jørgensen, F.E. *How to Measure Turbulence with Hot-Wire Anemometers: A Practical Guide*; Dantec Dynamics A/S: Skovlunde, Denmark, 2001.
27. Durst, F. *Fluid Mechanics: An Introduction to the Theory of Fluid Flows*; Springer Science & Business Media: Berlin, Germany, 2008.
28. El-Gabry, L.A.; Thurman, D.R.; Poinsatte, P.E. *Procedure for Determining Turbulence Length Scales Using Hotwire Anemometry*; Technical Report, GRC-E-DAA-TN4063; National Aeronautics and Space Administration, Glenn Research Center: Cleveland, OH, USA, 2014.
29. Kurian, T.; Fransson, J.H. Grid-generated turbulence revisited. *Fluid Dyn. Res.* **2009**, *41*, 021403. [CrossRef]
30. Czwielong, F.; Floss, S.; Kaltenbacher, M.; Becker, S. Influence of a micro-perforated duct absorber on sound emission and performance of axial fans. *Appl. Acoust.* **2021**, *174*, 107746. [CrossRef]
31. Czwielong, F.; Becker, S. Controlled Inflow Turbulence-Aeroacoustic Interaction of Axial Fans with an Active Turbulence Grid. In Proceedings of the FAN 2022—International Conference on Fan Noise, Aerodynamics, Applications and Systems, Senlis, France, 27–29 June 2022. [CrossRef]
32. Czwielong, F.; Hruška, V.; Bednařík, M.; Becker, S. On the acoustic effects of sonic crystals in heat exchanger arrangements. *Appl. Acoust.* **2021**, *182*, 108253. [CrossRef]
33. Biedermann, T.M.; Czeckay, P.; Hintzen, N.; Kameier, F.; Paschereit, C.O. Applicability of aeroacoustic scaling laws of leading edge serrations for rotating applications. *Acoustics* **2020**, *2*, 579–594. [CrossRef]
34. Ocker, C.; Czwielong, F.; Geyer, T.F.; Chaitanya, P.; Merkel, M.; Becker, S. Permeable Structures for Leading Edge Noise Reduction. In Proceedings of the AIAA AVIATION 2021 FORUM, Virtual Event, 2–6 August 2021; p. 2192. [CrossRef]
35. Sharland, I., Jr. Sources of noise in axial flow fans. *J. Sound Vib.* **1964**, *1*, 302–322. [CrossRef]
36. Bommes, L. (Ed.) *Ventilatoren*; Vulkan-Verlag GmbH: Essen, Germany, 2003.
37. Van Veldhuizen, D.A.; Lamont, G.B. Evolutionary Computation and Convergence to a Pareto Front. In Proceedings of the Late Breaking Papers at the Genetic Programming 1998 Conference, Madison, WI, USA, 22–25 July 1998; pp. 221–228.
38. Lucius, A.; Hütter, S.; Dietrich, P.; Schneider, M.; Lehmann, M.; Geyer, T. Experimental and numerical investigation of axial fan aeroacoustics at disturbed inflow conditions. In Proceedings of the Fan 2018, International Conference on Fan Noise, Aerodynamics, Applications and Systems, CETIAT, Darmstadt, Germany, 18–20 April 2018.
39. Schneider, M.; Feldmann, C. Psychoacoustic evaluation of fan noise. In Proceedings of the Fan 2015 International Conference on Fan Noise, Technology and Numerical Methods, Lyon, France, 15–17 April 2015.